The magnetic moment of NiO nanoparticles determined by Mössbauer spectroscopy

2006 J. Phys.: Condens. Matter 18 4161

(http://iopscience.iop.org/0953-8984/18/17/005)

INSTITUTE OF PHYSICS PUBLISHING JOURNAL OF PHYSICS: CONDENSED MATTER

J. Phys.: Condens. Matter **18** (2006) 4161–4175 doi:10.1088/0953-8984/18/17/005

The magnetic moment of NiO nanoparticles determined by Mössbauer spectroscopy

C R H Bahl[1,2], M F Hansen[3], T Pedersen[1], S Saadi[1], K H Nielsen[1], B Lebech[2] and S Mørup[1]

[1] Department of Physics, Building 307, Technical University of Denmark, DK-2800 Kongens Lyngby, Denmark
[2] Materials Research Department, Building 227, Risø National Laboratory, DK-4000 Roskilde, Denmark
[3] MIC—Department of Micro and Nanotechnology, Building 345 East, Technical University of Denmark, DK-2800 Kongens Lyngby, Denmark

E-mail: morup@fysik.dtu.dk

Received 14 February 2006
Published 13 April 2006
Online at stacks.iop.org/JPhysCM/18/4161

Abstract

We have studied the magnetic properties of ^{57}Fe-doped NiO nanoparticles using Mössbauer spectroscopy and magnetization measurements. Two samples with different degrees of interparticle interaction were studied. In both samples the particles were characterized by high-resolution transmission electron microscopy and x-ray diffraction and found to be plate-shaped. Computer simulations showed that high-field Mössbauer data are very sensitive to the size of the uncompensated magnetic moment. From analyses of the Mössbauer spectra we have estimated that the size of the uncompensated magnetic moment is in accordance with a model based on random occupation of surface sites. The analyses of the magnetization data gave larger magnetic moments, but the difference can be explained by the different sensitivity of the two methods to a particle size distribution and by interactions between the particles, which may have a strong influence on the moments estimated from magnetization data.

(Some figures in this article are in colour only in the electronic version)

1. Introduction

NiO is an archetypal antiferromagnet and was one of the first materials in which antiferromagnetism was studied [1]. It has an fcc structure, with the spins arranged in alternating ferromagnetically ordered {111} planes, giving an antiferromagnetic ordering vector along the [111] direction, i.e. it is a so-called type II antiferromagnet. In bulk, the spins are confined to the [11$\bar{2}$] direction within the (111) plane [2]. Due to this spin structure, the exchange coupling to the nearest neighbours within the ferromagnetic planes is slightly larger than that to the nearest neighbours out of these planes. This exchange striction manifests itself

in NiO not being perfectly cubic but having a small contraction of the distance between the ferromagnetically ordered planes below the Néel temperature [3]. However, the difference in plane spacing is only about 0.1% at 300 K [3] and this deviation from cubic symmetry is in general ignored.

In a number of studies of nanoscale NiO it has been found that very small particles can have quite large magnetic moments [4–10]. Néel [11] suggested that this can be explained by the presence of uncompensated magnetic moments, and he considered three different situations for the number of uncompensated spins in small particles of an antiferromagnet. These general cases, also discussed in [6], give different numbers of uncompensated spins q depending on the model employed. If the uncompensated spins occur at random in a particle, a value of $q \approx n_s^{1/2}$ is found, where n_s is the number of spins. If the spins are arranged in ferromagnetically ordered layers stacked into a cube with an odd number of layers the value is $q \approx n_s^{2/3}$. Finally, if the structure is perfect except for spins missing at random on the surface, the value is $q \approx n_s^{1/3}$. From measurements of the relationship between the magnetic susceptibility and the particle size, Richardson *et al* [6] found a size dependence of the susceptibility with $q \propto n_s^{1/3}$, with a proportionality factor of about 4, but the shape of the particles was not mentioned. In the literature, it has often been assumed that the number of uncompensated spins is of the order of $n_s^{1/2}$. However, the model used to obtain this value, i.e. a random occupancy of the sites in the particle, would undoubtedly lead to severe crystallographic and magnetic disorder, but this is not observed in studies of, for example, nanoparticles of NiO [12] and α-Fe_2O_3 [13]. It therefore seems more realistic that the uncompensated moment has its main contribution from the surface. In the present work we have estimated the moments of plate-shaped NiO nanoparticles using high-field Mössbauer data and magnetization measurements.

2. Materials and methods

$Ni(OH)_2$ was chemically precipitated by mixing aqueous solutions of NaOH and $Ni(NO_3)_2{\cdot}6H_2O$. It was transformed to NiO by heating in atmospheric air at 300 °C for 3 h, as described in [14]. In order to enable Mössbauer spectroscopy, samples were made by the same procedure from $Ni(OH)_2$ doped with 0.5 at.% ^{57}Fe relative to Ni. The sample is from the same batch as the as-prepared sample of [14] displaying significant interparticle interaction. A second set of doped and undoped NiO samples displaying less interparticle interaction was prepared by grinding the as-prepared samples by hand in an agate mortar for 15 min. Earlier studies have shown that gentle grinding can significantly reduce interactions between nanoparticles [15].

^{57}Fe Mössbauer spectroscopy was performed on both the as-prepared and the ground sample using a source of ^{57}Co in a rhodium matrix. Spectra were recorded in a liquid helium cryostat at 6 K in zero applied field and in a magnetic field of 6 T applied parallel to the radiation direction. Temperature series from 80 to 295 K were recorded at zero applied field in a liquid nitrogen cryostat. The powder samples were diluted by mixing with boron nitride powder without grinding.

The samples were studied by high-resolution transmission electron microscopy (HRTEM) using a JEOL 3000 FEG microscope equipped with a Gatan 16 Mpix CCD camera. X-ray diffraction (XRD) was carried out at ambient conditions in a Philips PW 1820 diffractometer using the Kα radiation from a Cu anode. Magnetometry was performed using a LakeShore 7407 vibrating sample magnetometer (VSM), with a maximum field of 1.6 T. These measurements were carried out at temperatures from 80 to 300 K, using a liquid nitrogen cryostat. Samples of ~100 mg were measured in Teflon cups. The background signal from the empty cups was subtracted.

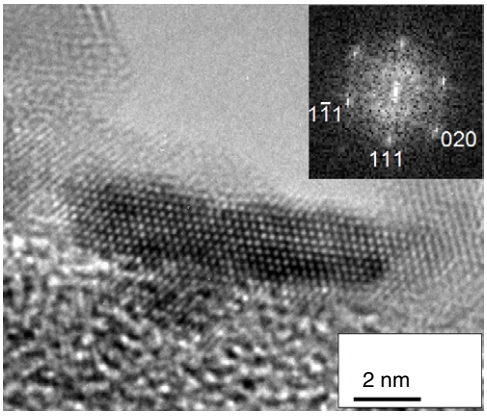

Figure 1. HRTEM image of a platelet-shaped NiO nanoparticle from the as-prepared sample, seen edge on. The inset is a Fourier transform of the image indicating how the (111) plane is parallel to the plate face. The plate face is seen to have an irregular surface.

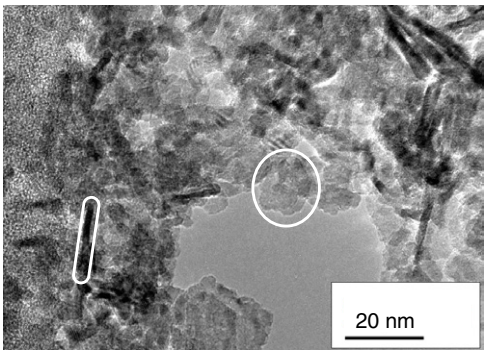

Figure 2. TEM image of the edge of an agglomerate of NiO nanoparticles in the as-prepared sample, showing how the platelet-shaped particles are found in random orientations. The two indicated platelets are oriented edge-on and face-on.

3. Results

3.1. Structure and morphology of the sample

Samples for HRTEM studies were prepared by suspending some of the powder in water and air drying a droplet on a grid. In both the ground and as-prepared samples the particles were found in 100–500 nm sized agglomerates. The particles are platelet-shaped particles, with {111} lattice planes as faces, as illustrated in figure 1 which shows a HRTEM image obtained from the as-prepared sample. Measuring the particle size in the as-prepared sample gave an average plate diameter of 13 $\pm$ 3 nm and an average thickness of 2.3 $\pm$ 0.4 nm. Here the uncertainties give the standard deviation of the size distributions. There is no obvious difference between images of the two samples. No interaction or orientation effects are observed in either sample, as the platelets are found with random orientations relative to each other throughout the agglomerates, as seen in figure 2.

XRD analysis showed that doping and grinding does not change the size or morphology of NiO samples [16]. Profile refinement using the FullProf software [17] was performed on the

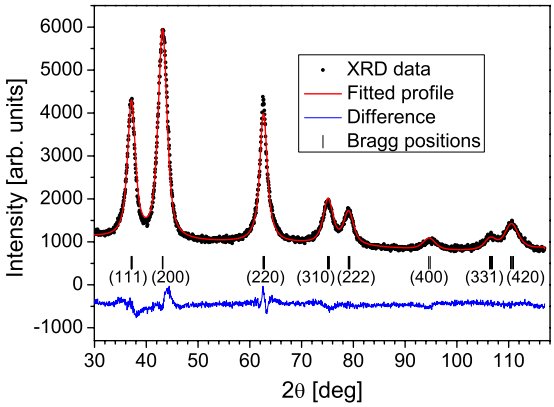

Figure 3. XRD spectrum from the as-prepared sample profile refined by the FullProf software, assuming a platelet particle shape. The refinement was done using a pseudo-hexagonal unit cell, as described in the text, but for clarity the conventional cubic indexing is used in the figure.

as-prepared undoped sample. The refinement showed that both samples consist of pure NiO with no visible trace of $Ni(OH)_2$ or other impurity phases. The refinement was done with the cubic unit cell and space group $Fm3m$, giving a lattice constant of $a = 4.194$ Å, which is slightly larger than the value of $a = 4.180$ Å found from the refinement of a spectrum recorded from a commercial bulk NiO powder but in accordance with the results of previous XRD studies of NiO nanoparticles [6, 18].

Assuming a spherical particle shape, the refined profile gave a particle diameter of 3.6 nm. From the knowledge gained from the TEM study, it seemed more realistic to fit the spectra assuming disc-shaped particles. In order for the software to distinguish between the four different ⟨111⟩ directions the cubic NiO unit cell was transformed to a pseudo-hexagonal one [19] with space group $R\bar{3}m$, the a and b axes in the (111) plane and the c axis along the [111] direction.

The fit of the spectrum of the as-prepared sample, assuming a platelet shape with the [111] direction perpendicular to the plate face, gave lattice parameters $a = 2.966$ Å and $c = 7.259$ Å compared to the values of $a = 2.955$ Å and $c = 7.246$ Å obtained in the bulk powder. The fit is shown in figure 3. It gave an estimated plate thickness of 2.3 nm and an estimated diameter of 7.9 nm. The diameter is smaller than that found by TEM, but the fit does not completely describe the narrow peak of the $(220)_{\text{cubic}} = (110)_{\text{hex}}$ reflection, which is in the disc plane. This will underestimate the diameter of the particles and is probably caused by the size distribution of the particles.

3.2. Mössbauer spectroscopy

Mössbauer spectra of the as-prepared and ground doped samples, recorded at temperatures from 6 to 295 K, are presented in figure 4. At low temperatures the spectra consist of magnetically split sextets. As the temperature increases the sextets gradually collapse into singlets, indicating fast superparamagnetic relaxation. At 295 K the spectra of both samples consist of a singlet with narrow line widths. The absence of quadrupole splitting shows that at least a large fraction of the ^{57}Fe atoms are in cubic environments as expected for a homogeneous substitution of ^{57}Fe in the Ni^{2+} sites in NiO in both samples. In the ground sample the sextet has almost collapsed at 105 K, whereas in the as-prepared sample the collapse is almost complete at

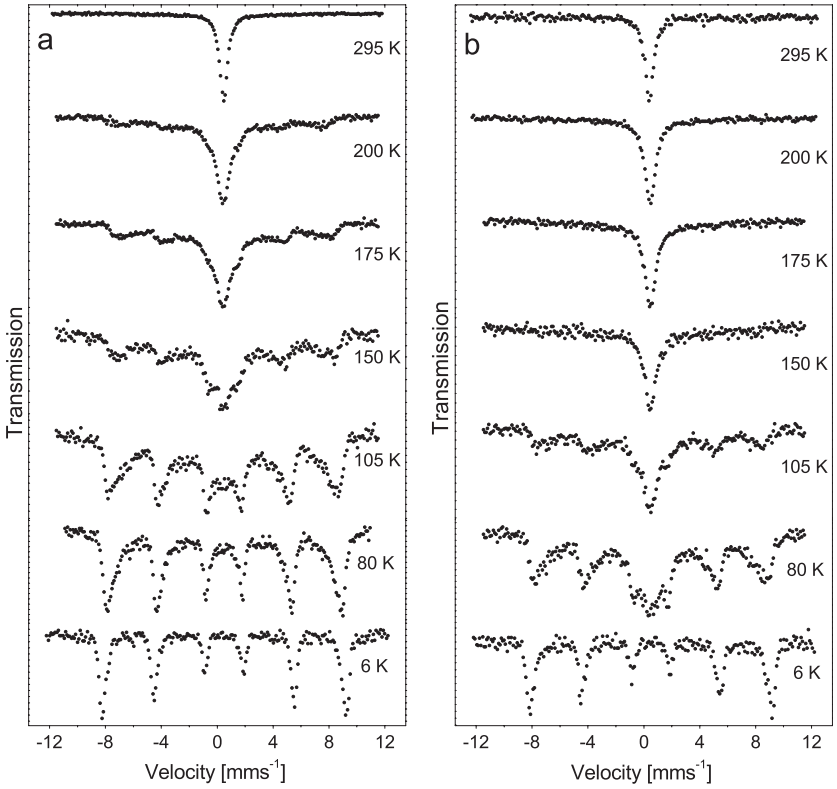

Figure 4. Mössbauer spectra of the ^{57}Fe-doped NiO nanoparticles recorded at temperatures in the range 6–295 K. (a) The as-prepared sample. (b) The ground sample.

around 175 K. Also, at $T \geqslant 80$ K the lines of the sextets are asymmetrically broadened due to hyperfine field distributions and relaxation effects. The asymmetric line broadening is typical for Mössbauer spectra of magnetic nanoparticles with some interparticle interaction due to exchange interaction between the particles [14, 20–22]. In [14] NiO particles from the same batch, but with significantly weaker interactions due to phosphate coating, were studied. In this sample, the blocking temperature, defined as the temperature where the singlet and sextet components have the same area, was about 50 K. In the present ground and as-prepared samples, the interaction raises the blocking temperatures to about 100 and 150 K, respectively.

Mössbauer spectra, obtained from both samples at 6 K in applied fields of 0 and 6 T, are shown in figures 5(a) and (b). The zero field spectra can be fitted with a single sextet. Line widths were constrained to be pair-wise identical. The Mössbauer parameters are given in table 1. The isomer shifts and magnetic hyperfine fields at low temperatures show that iron is present as Fe^{3+} in the high-spin state in both samples.

In ^{57}Fe Mössbauer spectroscopy, the areas of the lines in a magnetically split sextet (assuming a thin absorber) will scale as $3{:}p{:}1{:}1{:}p{:}3$, with

$$p = \frac{4\sin^2\theta}{2-\sin^2\theta}, \tag{1}$$

where θ is the angle between the total magnetic field at the nucleus and the incoming radiation. If the hyperfine fields of the particles in the sample are randomly oriented, the area ratio of

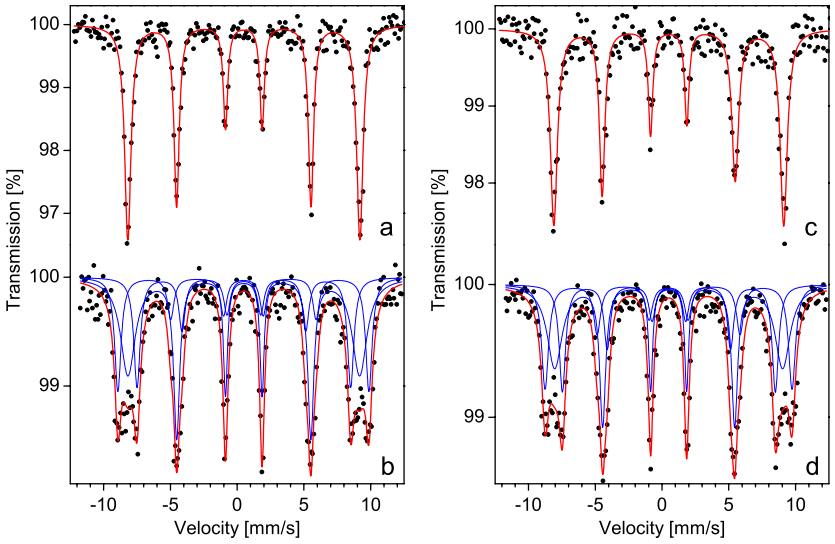

Figure 5. Mössbauer spectra of both samples of NiO nanoparticles doped with iron all recorded at 6 K. (a) The as-prepared sample recorded in zero applied field. (b) The as-prepared sample recorded in an applied field of 6 T. (c) The ground sample recorded in zero applied field. (d) The ground sample recorded in an applied field of 6 T. The small amount of iron in the samples is the reason for the poor statistics in the measured spectra. The thin lines (blue online) are the individual sextets, and the broader line (red online) is the sum of these.

Table 1. Parameters obtained from the fit to the 6 K Mössbauer spectra of NiO nanoparticles in zero applied field and an applied field of 6 T for both the as-prepared and the ground sample. The field is applied parallel to the propagation direction of the gamma rays. The line area parameters, p, for the sextets 2 and 3 in an applied field of 6 T were fixed according to the values of the total field at the nuclei as described in the text.

	B_{tot} (T)	Isomer shift (mm s^{-1})	Quadrupole shift (mm s^{-1})	Line area parameter p	Relative area of component (%)
As-prepared sample					
$B_{\mathrm{app}} = 0$ T					
Sextet 1	53.9(1)	0.50(2)	0.00(2)	2.1(2)	100
$B_{\mathrm{app}} = 6$ T					
Sextet 1	53.8(5)	0.50(3)	0.00	2.0(2)	53(3)
Sextet 2	49.6(4)	0.50(3)	0.00	1.44	24(3)
Sextet 3	58.3(4)	0.47(3)	0.00	1.09	23(3)
Ground sample					
$B_{\mathrm{app}} = 0$ T					
Sextet 1	53.4(1)	0.50(2)	0.00(2)	2.2(2)	100
$B_{\mathrm{app}} = 6$ T					
Sextet 1	53.0(5)	0.50(3)	0.00	1.7(2)	48(3)
Sextet 2	49.5(4)	0.51(3)	0.00	1.79	26(3)
Sextet 3	57.3(4)	0.49(3)	0.00	1.42	26(3)

the lines will be 3:2:1:1:2:3. Fitting the zero-field spectra obtained at 6 K with the area ratio 3:p:1:1:p:3 gave values of $p = 2.1(2)$ for the as-prepared sample and $p = 2.2(2)$ for the

ground sample, indicating that the particles in the samples are indeed close to being randomly oriented.

Application of a field of 6 T parallel to the propagation direction of the gamma rays results in a splitting of the spectra into more than one sextet (see figures 5(c) and (d)). The spectra were well fitted using three sextets, one with broad lines and an average hyperfine field close to that found in zero applied field, as expected for a powder of randomly oriented antiferromagnetic material. In the as-prepared sample, the other two have magnetic splittings about 4.3 T larger and smaller than found in zero applied field. In the ground sample, the two sextets have magnetic splittings about 3.9 T larger and smaller than found in zero applied field. The two sextets are similar to those found in high-field spectra of ferrimagnetic materials such as maghemite, in which atoms belonging to the two sublattices have hyperfine fields parallel and antiparallel to the applied field, respectively. Thus, the Mössbauer spectrum resembles that expected from a mixture of ferrimagnetic and antiferromagnetic material.

The fit of the spectrum of the as-prepared sample with the three sextets as described above reveals that the difference between the splittings of the 'ferrimagnetic' sextets (sextets 2 and 3) is (58.3(4)–49.6(4) T) = 8.7(6) T instead of 12 T as expected for a perfectly aligned ferrimagnetic material in an applied field of 6 T. The values of the total field at the nucleus, B_{tot}, the hyperfine field, B_{hf}, and the applied field, B_{app}, are related by the expression

$$B_{\mathrm{hf}}^2 = B_{\mathrm{tot}}^2 + B_{\mathrm{app}}^2 - 2B_{\mathrm{tot}}B_{\mathrm{app}}\cos\theta. \tag{2}$$

Thus, the magnitude of the magnetic splitting can be explained by imperfect alignment of the spins to the applied field and the angles θ can be calculated for each of the two sublattices. These angles also determine the area ratios of the lines according to equation (1). A model where all the spins in each sublattice are aligned at the same angle to the applied field is assumed. Iteratively fitting the spectrum with the three sextets keeping the area ratios in the two 'ferrimagnetic' sextets fixed to the values calculated from the splitting, and leaving it free in the 'antiferromagnetic' sextet, gives the parameters in table 1, and values of $\theta \approx 41°$ and $\theta \approx 133°$ for the two sublattices. The fit to the 'antiferromagnetic' part of the spectrum gave a line area parameter $p = 2.0(2)$. The line widths were constrained to be pair-wise identical. The FWHM of the lines in the the 'antiferromagnetic' component were found to increase from 0.4 to 1.3 mm s^{-1} towards the outer lines, yielding a FWHM of the field distribution for these corresponding to 4.0 T. The widths of the lines in the two 'ferrimagnetic' sextets were constrained to be identical and found to be around 0.6 mm s^{-1}. The quadrupole shifts were fixed to 0.00 mm s^{-1} in all the sextets in accordance with the result from the spectrum in zero applied field.

Similar results are found by fitting the ground sample in the same way, with a splitting of the ferrimagnetic sextets of 7.9(6) T. The widths of the lines were very close to those found in the as-prepared sample. The results of the fitting are also summarized in table 1.

3.3. Magnetometry

Hysteresis loops of the undoped as-prepared and ground samples were measured in the VSM in the temperature interval from 80 to 300 K. At 80 K there is a clear hysteresis, which diminishes as the temperature is increased and has completely disappeared at 200 K in both samples. The 80 and 200 K magnetization data are shown in figure 6, with the central parts of these hysteresis curves shown in the inset. Above the temperature where the hysteresis disappears and below the Néel temperature (≈460 K [12]) the particles are superparamagnetic. In this regime the specific magnetization of the ith particle may be described by a Langevin function in combination with

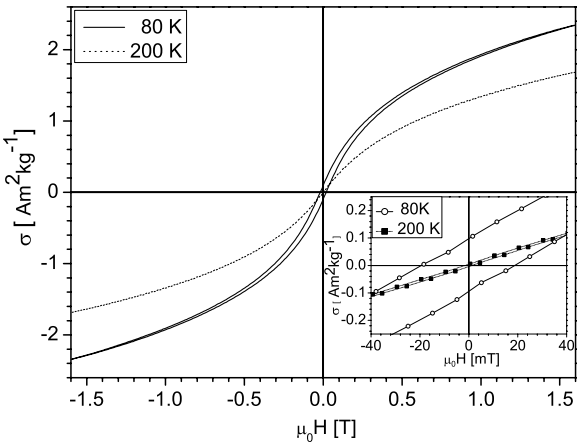

Figure 6. Hysteresis loops from the as-prepared sample at 80 and 200 K. The inset is a close up of the centre of the hystereses, showing the large remanence and coercivity of the particles at 80 K.

a linear term [6]:

$$\sigma_i = \frac{\mu_i}{m_i}\mathcal{L}\left(\frac{\mu_i B_{\text{app}}}{k_{\text{B}}T}\right) + \chi_{\text{A}}\frac{B_{\text{app}}}{\mu_0} \tag{3}$$

where $\mathcal{L}(x) = \coth(x) - \frac{1}{x}$ is the Langevin function, μ_i is the magnetic moment, m_i is the mass, χ_{A} is the antiferromagnetic mass susceptibility of the NiO, k_{B} is Boltzmann constant, μ_0 is the vacuum permeability and B_{app} is the applied field.

4. Discussion

4.1. Mössbauer data

When analysing the Mössbauer data, it must be realized that we do not directly observe the magnetic properties of the Ni^{2+} ions but obtain information on the substituted Fe^{3+} ions. It is reasonable to assume that the Fe^{3+} ions are randomly distributed among the two sublattices, such that the contribution to the net magnetization from the small number of Fe^{3+} ions is negligible. We also assume that the spins of the Fe^{3+} ions in otherwise defect-free environments are exchange coupled to the Ni^{2+} ions such that they are parallel (or antiparallel) to Ni^{2+} ions in the same layer. However, the requirement of charge balance presumably results in one cation vacancy for every two substituted Fe^{3+} ions. Therefore, some of the Fe^{3+} ions may have a vacancy in their near environments, and this may result in some local magnetic disorder. Also, the lack of neighbours creates non-cubic environments for Fe^{3+} ions at surface sites. However, the absence of quadrupole splitting in the superparamagnetic components indicates that a large fraction of the Fe^{3+} ions are in non-distorted cubic environments within the particles as expected for a homogeneous distribution of Fe^{3+} ions.

The fits of the 6 T Mössbauer spectra in both samples suggest that about half the Fe^{3+} spins are only weakly affected by the field, and the other half to some degree are aligned parallel or antiparallel with the field. Qualitatively, this may be explained by Néel's model for uncompensated spins in nanocrystals with even or odd numbers of layers with ferromagnetic order and alternating magnetization directions. In this model, particles with an even number of layers should behave as ideal antiferromagnets, whereas particles with an odd number of layers are expected to behave as ferrimagnets. Another possible explanation is that essentially

all particles have non-zero magnetic moments due to, for example, random occupation of sites in the surface layers. In such a model, the sublattice magnetization directions of all particles are expected to be strongly affected by the applied field. The 'antiferromagnetic' component in the 6 T spectrum may then be explained by Fe^{3+} ions, which are subject to strong localized spin-canting. Such a model with a ferrimagnetic component and a strongly canted component has been successfully used to explain Mössbauer data for MnZn ferrite [23] and for tin-doped maghemite and maghemite nanoparticles [24].

As the hyperfine field at a given site is antiparallel to the sublattice magnetization, application of a field to a ferrimagnetic material will lead to a predominance of hyperfine fields antiparallel to the applied field. Thus sextet 2 would be expected to have a larger area than sextet 3. However, within the uncertainty the areas of the two sextets do not differ. Therefore, the number of magnetic ions in the two sublattices differs only slightly. If the 'ferrimagnetic' component were due to particles with an odd number of defect-free layers, one should expect for the present particles with a thickness of ∼10 layers, that sextet 2 should have an area about 20% larger than sextet 3, assuming a small magnetic anisotropy, such that the spins align with the applied field. Since this is not the case, it is more likely that the second model, with more or less random occupation of surface sites and localized spin-canting, gives a better description of the sample. This is also in accordance with the HRTEM image (figure 1), which shows irregularities in the surface. Localized spin-canting may take place in environments with missing neighbour ions, i.e. around vacancies [25] and at some surface sites [26]. The canting angles depend primarily on the ratio between the exchange coupling constants to neighbouring ions [25].

If the applied magnetic field is too small to change the spin orientations of an antiferromagnetic material or strongly canted spins appreciably, it is simply added to the randomly oriented hyperfine fields and this results in a line broadening. Numerical integration of the vector sum of the applied field (6 T) and the hyperfine field at zero applied field for all orientations of a particle gives a broad distribution of hyperfine fields, that can be fitted with a broad Lorentzian centred around 53.6 T with a FWHM of 1.1 mm s^{-1}. This is close to the widths estimated from the fit of the 'antiferromagnetic' component in the 6 T spectra of 1.3 mm s^{-1} in both the as-prepared and ground samples.

In a classical mean-field model, the energy of an antiferromagnet with uniaxial anisotropy and an uncompensated magnetic moment may be written as (assuming low temperature, thus neglecting thermal effects) [27]

$$E = N_a S g \mu_B \big[B_E \xi \cos(\theta_a - \theta_b) - \tfrac{1}{2} B_A \cos^2(\theta_a - t) - \tfrac{1}{2} B_A \xi^2 \cos^2(\theta_b - t) - B_{app}(\cos\theta_a + \xi \cos\theta_b) \big]. \quad (4)$$

Here S is the spin of the individual ions and N_a and $N_b = \xi N_a$ ($\xi \leqslant 1$) are the numbers of spins in the two sublattices. B_E, B_A and B_{app} are the exchange, anisotropy and applied fields, respectively. In bulk NiO there are two magnetocrystalline contributions to the anisotropy: an out-of-plane anisotropy which keeps the spins in an easy plane, and a much weaker in-plane anisotropy keeping the spins in a direction within this plane [2]. As the out-of-plane anisotropy is much larger than the in-plane anisotropy our model will consider spins confined to the plane, i.e. with an infinite out-of-plane anisotropy. The in-plane anisotropy field is given by $B_A = \frac{K}{M} = \frac{2\kappa S}{g\mu_B}$, where K is the anisotropy energy density, M is the sublattice magnetization and κ is the single ion anisotropy energy. It is assumed that all three fields are constant everywhere within the particle. θ_a, θ_b are the angles between the two sublattice magnetization directions and the applied field, and t is the angle between the in-plane anisotropy field of the particle (the easy axis) and the applied field.

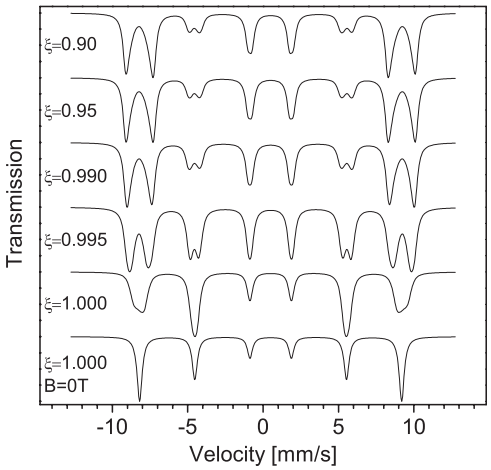

Figure 7. Simulated Mössbauer spectra of ideal antiferromagnetic particles with uncompensated spins. All spectra are normalized to the same maximum absorption. The spectra are simulated with exchange and anisotropy fields as described in the text, and an applied field of 6 T. The values of ξ are indicated. The bottom spectrum was simulated for zero applied field and $\xi = 1.000$.

We have simulated Mössbauer spectra using this model. We used the bulk value of the exchange field $B_E = 980$ T [2], and the applied field was set to $B_{app} = 6$ T as in the Mössbauer spectroscopy experiment. The in-plane anisotropy field $B_A = 0.014$ T was derived from the anisotropy constant found from the temperature dependence of the magnetic hyperfine splitting of very weakly interacting particles at low temperatures, as described in [22]. It is clear that regardless of the value of ξ, the exchange field will dominate, so the two sublattices will be very close to being antiparallel. In the perfect antiferromagnetic case, where $\xi = 1$, a moderate applied field cannot compete with the exchange field and the spin directions are mainly governed by the anisotropy field. However, only a small difference in the size of the total spins of the two sublattices can result in $B_{app}(1 - \xi) > B_A$, and then the applied field will dominate the alignment of the spins for all directions of the anisotropy field. In the regime where $B_A \approx B_{app}(1 - \xi)$, i.e. when $\xi \approx 0.990$, both the applied field and the anisotropy field will strongly influence the spin directions. For each orientation of the easy axis, the spin directions giving the lowest energy were used to generate a Mössbauer spectrum. These spectra were weighted by $\sin t$ and added to cover all orientations of the anisotropy field. Figure 7 shows Mössbauer spectra simulated by this procedure for values of ξ between 0.900 and 1.000 in an applied field of 6 T. A spectrum with zero applied field is also shown for comparison. As expected, the spectrum changes drastically above $\xi \approx 0.99$. Here the lines broaden, especially the pairs of lines in lines 1 and 6, and the separation between the two sextets changes.

Lorentzians have been fitted to the series of simulated spectra with varying ξ. The difference in the magnetic hyperfine splitting between the two sextets is plotted in figure 8(a) and the average areas of line pairs in lines 2 and 5 are plotted in figure 8(b). Using figure 8(a) the hyperfine field splittings measured in the experimental spectra give values of $\xi = 0.993(1)$ and 0.995(1) in the as-prepared and ground samples, respectively. The simulated spectra with $\xi = 0.993$ and 1.000 have been added. Overlaying this sum of spectra with the experimentally measured spectrum of the as-prepared sample gives a reasonably good agreement between the two, as illustrated in figure 9(a). The same is also true when adding simulated spectra with $\xi = 0.995$ and 1.000 and overlaying this with the spectrum from the ground sample (see figure 9(b)).

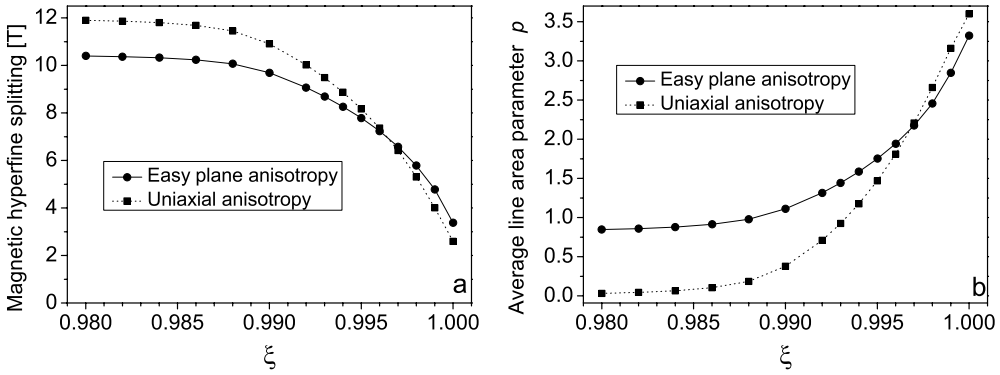

Figure 8. Parameters obtained by fitting Lorentzian line shapes to the simulated Mössbauer spectra as a function of the fraction of uncompensated moment. In both figures data are shown for the model in which the spins are confined to a plane with an easy direction (full line) as well as one assuming uniaxial anisotropy (dotted line). (a) The magnetic hyperfine field splitting between the two 'ferrimagnetic' sextets. (b) The average line area parameter, i.e. the area of lines 2 and 5.

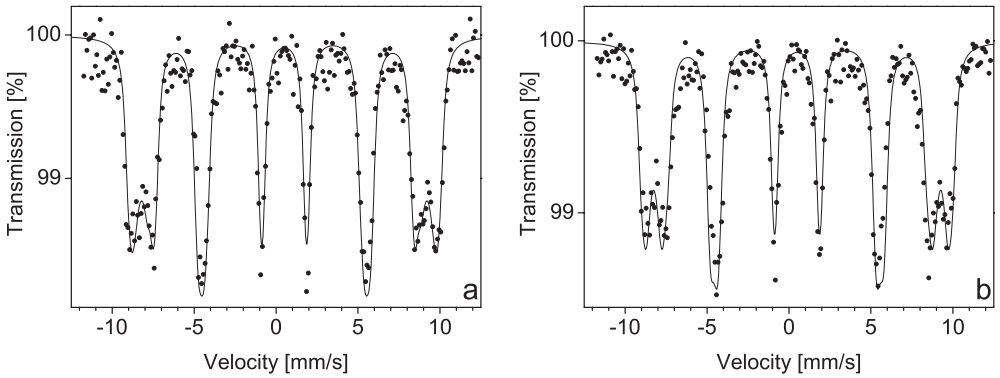

Figure 9. Overlay of the experimental data and the simulated spectra for both samples. (a) Simulated spectrum for the as-prepared sample consisting of the sum of a spectrum with $\xi = 1.000$ and one with $\xi = 0.993$. (b) Simulated spectrum for the ground sample consisting of the sum of a spectrum with $\xi = 1.000$ and one with $\xi = 0.995$.

Thus, the Mössbauer data can be explained by a model for an antiferromagnet with an easy plane anisotropy and uncompensated spins corresponding to about $(1 - \xi) = 0.005(1)$ and $(1 - \xi) = 0.007(1)$ for the as-prepared and ground samples, respectively, in addition to a number of ions with strong local spin-canting in both samples.

In nanoparticles the anisotropy is dominated by other contributions than in the bulk, such as, for example, surface anisotropy. In numerous studies of different magnetic nanoparticles it has been found that a simple uniaxial anisotropy (as in (4)) gives a good description of the magnetic properties. The simulated Mössbauer spectra have also been simulated using a model with uniaxial anisotropy, i.e. with zero out-of-plane anisotropy. The splittings of the sextets and average line area parameters obtained from this calculation are also presented in figures 8(a) and (b). It can be seen that at the relevant splittings the two models give similar values of the uncompensated moment.

4.2. Magnetization data

The VSM data, obtained above the blocking temperature, were first fitted assuming only one size of the magnetic moment, i.e. using (3) with $\sigma = N\sigma_i$, where N is the number of particles in the sample. However, the parameters obtained from these fits were apparently not reliable. For example, the value of χ_A was about seven times larger than the bulk value in both samples, although earlier experimental studies suggest that it is independent of particle size [6], and it was found to decrease with increasing temperature, which is opposite to the expected behaviour of an antiferromagnetic material. Further, the estimated average particle size in both samples was about seven to eight times larger than that found by electron microscopy, and the number of particles per gram apparently decreased with increasing temperature. It thus seemed likely that the contributions to the magnetization from the particles with the smallest moments could be well fitted with a straight line, and therefore the Langevin contributions from these particles were in practice indistinguishable from the linear term in (3). Silva *et al* [28] have recently pointed out that fitting magnetization data in this way can result in an apparent increase of the magnetic moment with temperature, because the size distribution is not correctly taken into account.

Another possible way of fitting the VSM data could be to fix the value of χ_A to the bulk value and fit the magnetization curves with a distribution of magnetic moments. However, unless the magnetic anisotropy is negligible compared to the Zeeman energy, it will give rise to deviations of the magnetization curves from Langevin functions [29, 30]. In nanoparticles with small magnetic moments, the deviations may be significant, and therefore the estimated moment distributions will not be reliable. To circumvent these complications, we have instead analysed the low-field data and estimated the initial susceptibility, which is independent of the anisotropy in samples with a random orientation of the easy axes [29–31]. For small applied fields, the magnetization of an assembly of nanoparticles can be approximated by

$$\sigma \approx \frac{1}{m}\sum_{i=1}^{N}\frac{\mu_i^2 B_{\mathrm{app}}}{3k_{\mathrm{B}}T} + \chi_{\mathrm{A}}\frac{B_{\mathrm{app}}}{\mu_0} = \frac{nB_{\mathrm{app}}}{3k_{\mathrm{B}}T}\langle\mu^2\rangle + \chi_{\mathrm{A}}\frac{B_{\mathrm{app}}}{\mu_0}. \tag{5}$$

Here m is the mass of the sample, and n is the number of particles per gram. The initial mass susceptibility is given by

$$\chi_{\mathrm{g}} = \frac{\mu_0\sigma}{B_{\mathrm{app}}} = \frac{n\mu_0}{3k_{\mathrm{B}}T}\langle\mu^2\rangle + \chi_{\mathrm{A}}. \tag{6}$$

We assumed that χ_A has a bulk value of 1.1×10^{-7} m^3 kg^{-1} in accordance with the results of an earlier study [6]. χ_A increases by about 10% from 160 to 300 K [32], but as χ_g was found to be $1.30(2)\times10^{-6}$ m^3 kg^{-1} $\gg \chi_A$ at 300 K in the as-prepared sample, the exact value of χ_A is not significant. Assuming the particle volume found by TEM ($\sim$300 nm^3), we arrive at an average of the squared moment of $\langle\mu^2\rangle \approx 2.74\times10^5\ \mu_B^2$ at 300 K in the as-prepared sample. For a lognormal distribution of the moments with a standard deviation between $\sigma_{\ln} = 0.4$ and 0.8 we have found that $\sqrt{\langle\mu^2\rangle}$ is between $1.1\langle\mu\rangle$ and $1.3\langle\mu\rangle$. Because the sublattice magnetization, and thus the measured moment of the NiO particles, decreases with increasing temperature [12], the low-temperature moment of the particles is about 25% larger than that measured at 300 K. Thus these two corrections counteract each other, depending on $\sigma_{\ln}$. Hence, we arrive at an average uncompensated moment of $\langle\mu\rangle \approx 520\ \mu_B$ corresponding to $\approx$260 Ni^{2+} ions each with an effective moment of $\mu_{\mathrm{eff}} = g\mu_B S = 2\ \mu_B$. Thus, the fraction of uncompensated spins $(1-\xi)$ corresponds to around 0.032 of the Ni^{2+} ions in one of the sublattices in the as-prepared sample. Note that whereas q denotes the fraction of uncompensated moment relative to the total number of ions, $(1-\xi)$ gives the fraction of uncompensated spins relative to the number of spins in one sublattice. In the ground sample a value of $\chi_g = 0.90(2)\times10^{-6}$ m^3 kg^{-1} was

found, yielding $\langle\mu^2\rangle \approx 1.83 \times 10^5\ \mu_B^2$ at 300 K. This gives a moment of $\langle\mu\rangle \approx 430\ \mu_B$ corresponding to a fraction of uncompensated spins, $(1 - \xi)$, of about 0.026.

There may be several reasons for the larger values of the uncompensated moments found by magnetometry compared to those obtained from the Mössbauer data. One reason may be that whereas the signal in Mössbauer spectroscopy is weighted by the volume of the particles, in magnetometry the signal is weighted by the moment. If there is a particle size distribution, and the moment of the small particles is larger than that of the large particles, a larger uncompensated moment will be observed by magnetometry than by Mössbauer spectroscopy. Another reason for this deviation may be magnetic interactions between the particles, especially in the as-prepared sample. Suppose the sample consists of clusters of strongly interacting particles, each containing N_c particles of moment μ_p. Then an analysis based on (5) according to the procedure described above and using as n the number of particles (not clusters) per gram will result in an estimate of the average of the squared moment of $\langle\mu^2\rangle \approx N_c\langle\mu_p^2\rangle$. Thus the calculated value of the uncompensated moment will be larger than the real value by a factor of $\sqrt{N_c}$. In fact, as mentioned above, the Mössbauer data in figure 4 show that there are indeed significant interactions between the particles in the as-prepared sample. In the ground sample the interparticle interactions are significantly less, but still present. As described above, a sample with negligible interaction has been prepared by coating separated particles with phosphate. However, the amount of phosphate compared to NiO and is not known. Further, the magnetic properties of the phosphate and a possible iron–phosphate interface layer are not known, so magnetization measurements on this sample would not be reliable. Mössbauer spectra from the sample contained a doublet component, presumably due to an iron–phosphate interface layer, that splits up into a sextet at low temperatures, making the sample unsuited for the high-field low-temperature experiments. As the effective fields from the interactions are weak compared to the applied field of 6 T, the value of the uncompensated moment, derived from the high-field Mössbauer spectrum, is only weakly affected by interactions between the particles. Thus, it is reasonable to assume that the uncompensated magnetic moments are of the order of 0.6% of the number of spins in one sublattice, as estimated from the Mössbauer data.

Thermoinduced magnetization has been proposed to explain the increase in the magnetic moment with temperature observed in nanoparticles of some antiferromagnetic materials [33, 34]. Applying the expression derived in [33] for this effect in a perfect antiferromagnet gives a moment of $\approx$100 μ_B at 300 K using the value of the in-plane anisotropy constant given below. Therefore, this contribution does not seem to be of major importance in the present NiO nanoparticles.

Using the particle size and shape obtained from TEM, we found that if the uncompensated magnetic moment were due to random occupation of surface sites, the number of uncompensated spins, $(1 - \xi)$, should be of the order of 0.003. This is in reasonable agreement with the values estimated from Mössbauer data. If the uncompensated moment were due to random occupation of sites throughout the particles one should expect a number of uncompensated spins, $(1 - \xi)$, of the order of 0.016, and if the particles consisted of even or odd numbers of defect-free planes, one would expect a number of uncompensated spins, $(1 - \xi)$, corresponding to about 20% of the number of spins in one sublattice. Thus, the data support the model with random occupation of surface sites. It is, however, likely that other effects, related to, for example, surface steps and localized spin-canting, also influence the size of the uncompensated moment. For spherical NiO nanoparticles simulations have shown that the magnetic structure may be more complex than the bulk magnetic structure [7, 35] and such phenomena may also be present in plate-shaped particles. However, neutron diffraction data from NiO nanoparticles prepared in the same way as the present samples were in accordance with a magnetic structure identical to that of bulk NiO [12].

Within the uncertainty, the two values of the uncompensated moment obtained from the Mössbauer data are the same, indicating that the interparticle interactions do not affect the uncompensated moment. Magnetization measurements gave two values that are clearly different, indicating varying degrees of clustering of the particles in the two samples as expected from the temperature series of Mössbauer data.

5. Conclusion

We have shown that high-field Mössbauer data are very sensitive to the magnitude of the uncompensated magnetic moment in nanoparticles of antiferromagnetic materials. This technique can be used to quantify the uncompensated magnetic moments in magnetic nanoparticles. Thus, we have found that the uncompensated magnetic moments in NiO nanoparticles correspond to about 0.7(1)% and 0.5(1)% of the number of Ni^{2+} ions in one sublattice in an as-prepared and a ground sample, respectively. The two samples display varying degrees of interparticle interaction. The measured moments are close to what is expected for a random occupation of surface sites in both samples, indicating that this is the main contribution to the uncompensated moment independent of interparticle interactions.

The analysis of the results of the magnetization measurements for the NiO particles showed that it is not straightforward to estimate the uncompensated moment from magnetization data. This is because of the broad distribution of magnetic moments, the influence of the magnetic anisotropy and the interparticle exchange interactions in both samples. An estimate, based on the initial susceptibility, which is independent of the magnetic anisotropy, gave uncompensated moments of about 3.2% and 2.6% in the as-prepared and ground samples, respectively. The larger values, compared to those obtained from Mössbauer data, can be explained by interparticle interactions in both samples as well as a difference in the sensitivity of magnetization measurements and Mössbauer spectroscopy to a particle size distribution.

Acknowledgments

The work was supported by the Danish Technical Research Council through the framework programme Nanomagnetism. The authors are grateful to H K Rasmussen for assistance with the low-temperature Mössbauer spectroscopy measurements and to F Bødker and L Lilleballe for preparation of the particles.

References

[1] Shull C G, Strauser W A and Wollan E O 1951 *Phys. Rev.* **83** 333
[2] Hutchings M T and Samuelsen E J 1972 *Phys. Rev.* B **6** 3447
[3] Bartel L C and Morosin B 1971 *Phys. Rev.* B **3** 1039
[4] Richardson J T and Milligan W O 1956 *Phys. Rev.* **102** 1289
[5] Schuele W J and Deetscreek V D 1962 *J. Appl. Phys.* **33** 1136
[6] Richardson J T, Yiagas D I, Turk B, Forster K and Twigg M V 1991 *J. Appl. Phys.* **70** 6977
[7] Kodama R H, Makhlouf S A and Berkowitz A E 1997 *Phys. Rev. Lett.* **79** 1393
[8] Makhlouf S A, Parker F T, Spada F E and Berkowitz A E 1997 *J. Appl. Phys.* **81** 5561
[9] Berkowitz A E, Kodama R H, Makhlouf S A, Parker F T, Spada F E, McNiff E J Jr and Foner S 1999 *J. Magn. Magn. Mater.* **196/197** 591
[10] Ichiyanagi Y, Wakabayashi N, Yamazaki J, Yamada S, Kimishima Y, Komatsu E and Tajima H 2003 *Physica* B **329–333** 862
[11] Néel L 1961 *Comp. Rend.* **252** 4075
[12] Klausen S N, Lindgård P-A, Bødker F and Mørup S 2002 *Phys. Status Solidi* a **189** 1039
[13] Bødker F, Hansen M F, Koch C B, Lefmann K and Mørup S 2000 *Phys. Rev.* B **61** 6826

[14] Bødker F, Hansen M F, Koch C B and Mørup S 2000 *J. Magn. Magn. Mater.* **221** 32
[15] Xu M, Bahl C R H, Frandsen C and Mørup S 2004 *J. Colloid Interface Sci.* **279** 132
[16] Bahl C R H and Mørup S 2006 *Nanotechnology* submitted
[17] http://www-llb.cea.fr/fullweb/
[18] Fiévet F, Germi P, de Bergevin F and Figlarz M 1979 *J. Appl. Crystallogr.* **12** 387
[19] Rodoc D, Spasojevic V, Kusigerski V, Tellgren R and Rundlof H 2000 *Phys. Status Solidi* b **218** 527
[20] Hansen M F, Koch C B and Mørup S 2000 *Phys. Rev.* B **62** 1124
[21] Frandsen C and Mørup S 2003 *J. Magn. Magn. Mater.* **266** 36
[22] Mørup S, Frandsen C, Bødker F, Klausen S N, Lefmann K, Lindgård P-A and Hansen M F 2002 *Hyperfine Interact.* **144/145** 347
[23] Anhøj T A, Bilenberg B, Thomsen B, Damsgaard C D, Rasmussen H K, Jacobsen C S, Mygind J and Mørup S 2003 *J. Magn. Magn. Mater.* **260** 115
[24] Helgason Ö, Rasmussen H K and Mørup S 2006 *J. Magn. Magn. Mater.* doi:10.1016/j.jmmm.2005.09.036
[25] Mørup S 2003 *J. Magn. Magn. Mater.* **266** 110
[26] Kodama R H, Berkowitz A E, McNiff E J Jr and Foner S 1996 *Phys. Rev. Lett.* **77** 394
[27] Pankhurst Q A 1991 *J. Magn. Magn. Mater.* **101** 291
[28] Silva N J O, Amaral V S and Carlos L D 2005 *Phys. Rev.* B **71** 184408
[29] Hanson M, Johansson C and Mørup S 1993 *J. Phys.: Condens. Matter* **5** 725
[30] Garcia-Palacios J L 2000 *Adv. Chem. Phys.* **112** 1
[31] Madsen D E, Mørup S and Hansen M F 2006 *J. Magn. Magn. Mater.* doi:10.1016/j.jmmm.2005.11.033
[32] Singer J R 1956 *Phys. Rev.* **104** 929
[33] Mørup S and Frandsen C 2004 *Phys. Rev. Lett.* **92** 217201
[34] Mørup S and Hansen B R 2005 *Phys. Rev.* B **72** 24418
[35] Lindgård P-A 2003 *J. Magn. Magn. Mater.* **266** 88